Fine-Tuning Property Domain Weighting Factors and the Objective Function in Force Field Parameter Optimization

Robin Strickstrock[a], Alexander Hagg[a], Marco Hülsmann[b], Karl N. Kirschner[b], Dirk Reith[a,*]

[a]*Department of Engineering and Communication (DEC), University of Applied Sciences Bonn-Rhein-Sieg, Grantham-Allee 20, 53757 Sankt Augustin, Germany*
[b]*Department of Computer Science (CS), University of Applied Sciences Bonn-Rhein-Sieg, Grantham-Allee 20, 53757 Sankt Augustin, Germany*

Abstract

Force field (FF) based molecular modeling is an often used method to investigate and study structural and dynamic properties of (bio-)chemical substances and systems. When such a system is modeled or refined, the force field parameters need to be adjusted. This force field parameter optimization can be a tedious task and is always a trade-off in terms of errors regarding the targeted properties. To better control the balance of various properties' errors, in this study we introduce weighting factors for the optimization objectives. Different weighting strategies are compared to fine-tune the balance between bulk-phase density and relative conformational energies (RCE), using n-octane as a representative system. Additionally, a non-linear projection of the individual property-specific parts of the optimized loss function is deployed to further improve the balance between them. The results show that

---

*Corresponding author.
E-mail address:* dirk.reith@h-brs.de

the overall error is reduced. One interesting outcome is a large variety in the resulting optimized force field parameters (FFPARAMS) and corresponding errors, suggesting that the optimization landscape is multi-modal and very dependent on the weighting factor setup. We conclude that adjusting the weighting factors can be a very important feature to lower the overall error in the FF optimization procedure, giving researchers the possibility to fine-tune their FFs.

Keywords: force field models; Lennard-Jones parameters, multiscale parameterization; local optimization; gradient-based optimization; weighting factors; objective function; non-linear projection;

1. Introduction

Over the past decades, computer-based molecular simulations have gained an increasingly important role in many scientific fields, for example, in material, (bio-)chemical, and pharmaceutical sciences. They are used to model structural properties or dynamic processes of diverse molecules and provide insight into the modeled molecular system at an atomistic level of detail and a fine temporal resolution. Commonly used methods are, for instance, molecular mechanic (MM) and molecular dynamic (MD) simulations. They are based on parameterized potential functions, called FF, that model the interactions between the atoms, molecules, or particles. The quality of the molecular simulations strongly depends on the used FF and the deployed FFPARAMS. Numerous good FF, usually including dedicated FFPARAMS for different applications, are available and have been developed over the past decades. Examples include General AMBER Force Field (GAFF) [1]

2

for small organic molecules compatible with Amber's [2] biological force fields, the very recent Amber-consistent small molecule FF developed by Xue et. al.[3], CHARMM general force field (CGENFF) [4] for bio- and drug-like molecules (an extension of the CHARMM [5, 6] force field and simulation tool), and optimized potentials for liquid simulations force field (OPLS) [7, 8] for liquids, organic molecules and peptides. Another well-established example is the Open Force Field Initiative (OPENFF) [9, 10, 11] using the SMIRKS-native Open Force Field (SMIRNOFF) [12] in combination with their versatile simulation toolkit called OpenMM [13]. A more detailed overview and discussion of recent FF development is provided by He et al. [14].

When optimizing FFPARAMS, usually the bonded interactions are fitted to quantum mechanic (QM) calculations of energies, frequencies and structures, while the van der Waals (VDW) parameters are optimized towards experimental quantities like densities or heat of vaporization [7]. The electrostatic terms are typically parameterized to reproduce QM electrostatic potentials [15, 16] or energies of water-molecule interactions [17]. Many of the available FFPARAMS optimization methods are either not automated or treat the optimization objectives sequentially, instead of simultaneously. To address the latter, we introduced a multiscale optimization workflow that simultaneously optimizes Lennard-Jones parameters (LJPARAMS) (i.e. σ_C, σ_H, ϵ_C and ϵ_H) towards different property domains (i.e. single-molecule or atomistic properties and multi-molecular properties) [18]. It was shown that the relative conformational energies (RCE) reproduction of n-octane could be significantly improved with a minimal reduction in the accuracy of its bulk-phase density. Herein, a modified approach is presented that provides

3

more control over the balancing of the optimized properties, improving the accuracy of the density calculations, while maintaining the RCE reproduction quality. This is achieved by a non-linear projection (NLP) of the individual property-specific parts of objective function and adapting their weighting factors (WFs). Four different approaches are investigated to determine the intra-domain WFs (i.e. those used within the same property domain). Additionally, inter-domain property balancing is introduced. Using this technique, the balance between the various properties subject to optimization is finely tuned. Both intra- and inter-domain balancing are combined with the NLP approach of the loss function's components. Finally, we present the best set of optimized FFParams, improving the previously achieved results [18]. We also show that different weighting factors result in different parameter sets, corresponding to different minima in the objective function landscape, indicating that FFParams optimization not only is a multiobjective but also a multi-modal problem and should be treated as such.

2. Methodology

To quantify the error of the parameter optimization, the following loss function $F(x)$ is defined [18]:

$$F(x) = \sum_{i=1}^{n} \omega_i^{\mathrm{MM}} \left(\frac{f_i^{\mathrm{QM}} - f_i^{\mathrm{MM}}(x)}{f_i^{\mathrm{QM}}} \right)^2 + \sum_{j=1}^{m} \omega_j^{\mathrm{MD}} \left(\frac{f_j^{\mathrm{exp}} - f_j^{\mathrm{MD}}(x)}{f_j^{\mathrm{exp}}} \right)^2 \quad (1)$$

The loss function is dependent on the force field parameters x and includes properties from different domains (i.e. the bulk-phase density and the RCE). The simulation results $f_i^{\mathrm{MM}}(x)$ and $f_j^{\mathrm{MD}}(x)$ originate from MM

4

minimization and MD calculation, respectively, and are dependent on the force field parameters x. They are subtracted from the particular property target values f_i^{QM} and f_j^{exp}, which are, for example, obtained by experiments. They are divided by the target values to get the relative deviations, squared to eliminate the sign, and scaled by a weighting factor ω. The target values consist of f_i^{QM}, $i = 1, \ldots, n$, containing the i-th RCE obtained from QM calculations (i.e. a single-molecular target property). For this work there are 96 unique RCE of n-octane ($n = 96$) that are obtained at an MP2.5/AVTZ theory level [19]. The f_j^{exp}, $j = 1, \ldots, m$, part contains the j-th experimentally obtained bulk-phase density (i.e. a multi-molecular target property). In this work, n-octane's bulk-phase density at $293.13\,\mathrm{K}$ and $1\,\mathrm{bar}$ pressure is used [20]. The associated WFs are ω_i^{MM} and ω_j^{MD}, which allows control of the relative importance of the optimization objectives. The number of individual properties in each domain is denoted with n and m. Note that any number of additional properties can be added to the optimization by adding a suitable term to the loss function.

2.1. Determining the Weighting Factor

For fine-tuning the WFs two aspects are considered. First, the **intra-domain** distribution of the WFs and second, their **inter-domain** balancing. The former concentrates on the distribution of the WFs values for one property independently from the other properties – for example assigning values for every ω_i^{MM} without concerning the values for ω_j^{MD} (see equation (1)). The latter takes the balance between the overall weights of the target properties from different domains (i.e. $\sum_i \omega_i^{\mathrm{MM}}$ vs. $\sum_j \omega_j^{\mathrm{MD}}$) into account.

Herein four approaches for the intra-domain weight balancing are pre-

5

sented: "uniformly distributed WFs", "linearly decreasing WFs", "exponentially decreasing WFs" and "stepwise decreasing WFs" (see figure 1), which are discussed in the following sections alongside the inter-domain balancing approach.

Because the RCE are the energies relative to the structure with the lowest energy and, by common convention, the lowest energy conformation is assigned the relative energy value of 0. Consequently, the difference between the simulation result and the target value is always 0 for this conformation and the corresponding weight ω_1^{MM} is also set to 0 in every approach. By setting $\omega_1^{\text{MM}} = 0$, it is ensured that the total amount of weight assigned for this property (i.e. $\sum_i \omega_i^{\text{MM}}$) is distributed among the non-zero RCE. Note that intra-domain balancing is not applied to the density WFs, because for this property domain herein only one value is used and thus a balancing is unnecessary.
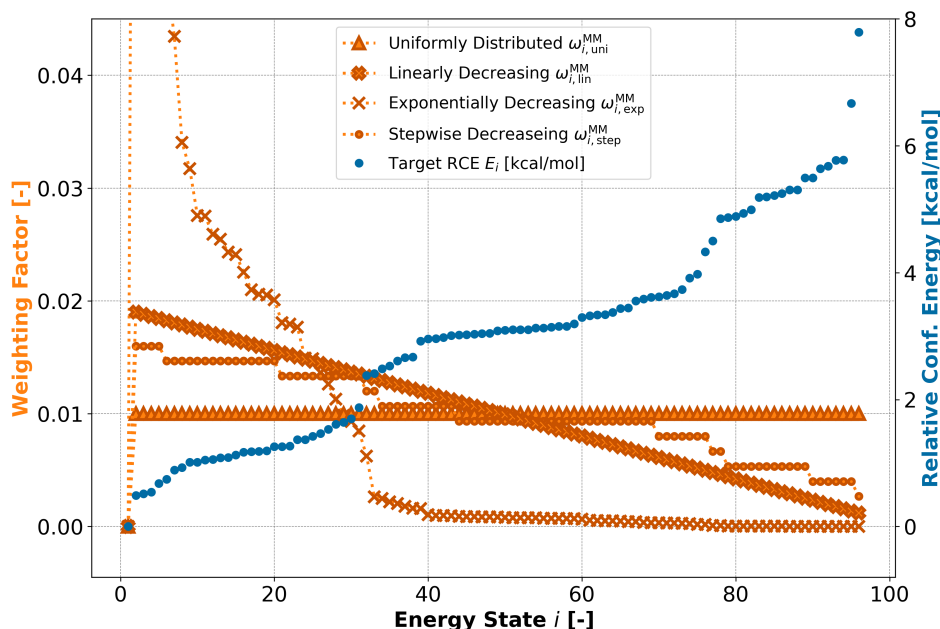
6

Figure 1: Examples for the four different intra-domain balancing approaches for the RCE WFs (orange graphs). Additionally, for every ω_i^{MM} the corresponding RCE is plotted (blue). <u>Note</u> that the highest values for $\omega_{i,\exp}^{\mathrm{MM}}$ are cut off because this figure aims to illustrate the trend of the WFs. For that purpose the exact values of every ω_i^{MM} have a low priority and, additionally, can vary based on the optimization problem and inter-domain balancing setup.

2.1.1. Uniform Distribution

The uniform distribution scheme assigns the same value to each RCE weighting factor. While simplistic in its implementation, this approach does not follow the chemical reasoning that in a real bulk-phase system of n-octane – at a given temperature and pressure – the possible conformations will not be equally populated, and are thus not equally important for the simulation

7

modeling. This approach was used in previous work [18] and serves as a baseline to compare the other approaches to.

The allocation of the uniform distribution WFs to n-octane's RCE is visualized in figure 1, where every factor ω_i^{MM} for $i = 2, \ldots, n$ is assigned the same value. The WFs corresponding to each of the RCE are calculated using the following equation:

$$
\begin{aligned}
\omega_{i,\mathrm{uni}}^{\mathrm{MM}} &= \frac{1}{(n-1)} \cdot b, \quad i = 2, \ldots, n \\
\omega_{1,\mathrm{uni}}^{\mathrm{MM}} &= 0
\end{aligned}
\tag{2}
$$

Thereby, n is the total number of WFs (here: $n = 96$) and b is the overall amount of weight that is assigned to the property domain (i.e. $\sum_i^n \omega_{i,\mathrm{uni}}^{\mathrm{MM}} = b$; here: $b = 0.96$). Note that b can, in general, be freely chosen and is only dependent on the inter-domain balancing, (see section 2.1.5, which also explains why $b = 0.96$ and not just $b = 1$).

2.1.2. Linearly Decreasing Distribution

An alternative simplistic approach is to assign a linear relationship between the WFs and the RCE that better highlights the importance of the lower energy conformations. At room temperature and atmospheric pressure ($293.15\,\mathrm{K}$ and $1\,\mathrm{bar}$), higher-energy conformations are less likely to occur than lower-energy conformations. Thus, the WFs have been adapted to linearly decrease (i.e. $\omega_{i+1,\mathrm{lin}} = \omega_{i,\mathrm{lin}} - d$), while still preserving the overall value for all RCE WFs (i.e. $\sum_i \omega_{i,\mathrm{lin}}^{\mathrm{MM}} = 0.96$). Figure 1 shows the WFs calculated using equation (3). *Note*, that the WFs are linearly decreasing w.r.t. the energy state IDs (i.e. $i = 1, \ldots, n$) and not a linear function dependent on the RCE values.

8

$$\omega_{n,\text{lin}} = k$$

$$\omega_{n-r,\text{lin}} = \omega_{n-r+1,\text{lin}} + d, \quad r = 1, \dots, n-2$$

$$d = 2 \cdot \frac{b - ((n-1) \cdot k)}{(n-2) \cdot (n-1)} \tag{3}$$

$$\omega_{1,\text{lin}} = 0$$

Thereby, n is the total number of WFs (here: $n = 96$) and b is the overall amount of weight that is assigned to the property domain (i.e. $\sum_i^n \omega_{i,\text{lin}}^{\text{MM}} = b$; here: $b = 0.96$). k is a user-chosen value for the lowest weighting factor $\omega_{n,\text{lin}}$. It determines the slope of linearly decreasing WFs and how much weight is assigned to the other WFs, because the sum of all WFs can not exceed b. Furthermore, $k > 0$ and is chosen such, that the WFs clearly differ from the uniformly distributed WFs (here: $k = 0.001$).

2.1.3. Exponentially Decreasing Distribution

The exponentially decreasing WFs for the RCE follows an idea similar to the linearly decreasing WFs. In contrast, however, this approach is based on a Boltzmann distribution (see equation (4)) and is visualized in figure 1. This approach attempts to mimic the probability that a conformation occurs based on its internal energy in combination with the system's temperature. Thus, its importance for the parameter optimization is based on those properties.

$$\tilde{\omega}_{i,\text{exp}}^{\text{MM}} = \mathrm{e}^{-E_{\tilde{i}}(k_{\text{B}} \cdot T)^{-1}}$$

$$\omega_{i,\text{exp}}^{\text{MM}} = \tilde{\omega}_{i,\text{exp}}^{\text{MM}} \cdot \frac{b}{\sum_i^n \tilde{\omega}_{i,\text{exp}}^{\text{MM}}}, \quad i = 2, \dots, n \tag{4}$$

$$\omega_{1,\text{exp}}^{\text{MM}} = 0$$

9

Thereby, E_i is the i-th RCE (Note, that for E_i the units are converted from kcal/mol to joule), $k_B = 1.38064852 \cdot 10^{-23} \, \mathrm{m^2 \cdot kg \cdot s^{-2} \cdot K^{-1}}$ (Boltzmann's constant) and T the temperature (here: $T = 293.15 \, \mathrm{K}$). The number of WFs is n (here: $n = 96$) and b is the overall amount of weight that is assigned to the property domain (i.e. $\sum_i^n \omega_{i,\mathrm{exp}}^{\mathrm{MM}} = b$; here: $b = 0.96$). After calculating the unscaled WFs $\tilde{\omega}_{i,\mathrm{exp}}^{\mathrm{MM}}$ they are scaled such that $\sum_i^n \omega_{i,\mathrm{exp}}^{\mathrm{MM}} = b$, resulting in the actual WFs $\omega_{i,\mathrm{exp}}^{\mathrm{MM}}$.

2.1.4. Stepwise Decreasing Distribution

The underlying idea for a stepwise decreasing distribution of the WFs for the RCE is that room temperature introduces an energy of approximately $0.6 \, \mathrm{kcal \cdot mol^{-1}}$ to a system. Thus, the RCE are grouped into multiples of $0.6 \, \mathrm{kcal \cdot mol^{-1}}$ and every subsequent group, containing energetically higher RCE than the previous group, are weighted less because they are less likely to occur. They are calculated following equation (5) and are visualized in figure 1.

To calculate the stepwise decreasing WFs, first, the set $\mathcal{E}$ containing all RCE $e_1, \ldots, e_n$ is divided into subsets $\mathcal{A}_1, \ldots, \mathcal{A}_p$ containing the energies that are less or equal than multiples of the stepsize k (here: $k = 0.6 \, \mathrm{kcal \cdot mol^{-1}}$):

$$\mathcal{E} = \{e_2, \ldots, e_n\} = \cup_{q=1}^p \mathcal{A}_q$$
$$\mathcal{A}_q = \{e_i \in \mathcal{E} \,|\, (q-1) \cdot k < e_i \leq q \cdot k\}, \quad i = 2, \ldots, n$$

Where p is the number of different subsets $\mathcal{A}$. For every RCE e_i, the corresponding unscaled weighting factor $\tilde{\omega}_{i,\mathrm{step}}^{\mathrm{MM}}$ is assigned based on the subset $\mathcal{A}_q$ the RCE e_i is an element of. Thereby, the WFs corresponding to the RCE

10

with the lowest energy are assigned the highest value:

$$\tilde{\omega}_{i,\text{step}}^{\text{MM}} = p - (q - 1), \quad \forall i : e_i \in \mathcal{A}_q$$

Finally, the WFs $\tilde{\omega}_{i,\text{step}}^{\text{MM}}$ are scaled such that their sum equals the overall amount of weight that is assigned to the property domain b (here: $b = 0.96$), resulting in the scaled WFs:

$$\omega_{i,\text{step}}^{\text{MM}} = \frac{\tilde{\omega}_{i,\text{step}}^{\text{MM}}}{\sum_i^n \tilde{\omega}_{i,\text{step}}^{\text{MM}}} \cdot b$$

$$\omega_{1,\text{step}}^{\text{MM}} = 0$$

(5)

2.1.5. Inter-Domain Balancing

In the previous work [18] the summed values of the WFs of the two domains (i.e. $\sum_{i=1}^n \omega_i^{\text{MM}}$ vs. $\sum_{j=1}^m \omega_j^{\text{MD}}$) were equally weighted, putting no emphasis on either domain. In order to improve the force field for both domains, in this work different inter-domain weights are evaluated to re-balance the loss function. For example, by setting $\sum_{j=1}^m \omega_j^{\text{MD}} = 1.44$ (that herein simplifies to $\omega^{\text{MD}} = 1.44$) and $\sum_{i=1}^n \omega_i^{\text{MM}} = 0.48$, a re-balancing is reached that assigns 75% of the overall weight to the density, and thus is called "75-25". The different intra-domain balancing setups used herein are listed in section 2.4.

2.2. Non-linear Projection Of The Loss Function

A difficulty in this simultaneous multiscale optimization approach is that the loss function values for the different target domains might be poorly comparable. For example, the error for the RCE ($\text{err}_{\text{RCE}} \approx 10\% \ldots 100\%$) is approximately one to two orders of magnitude higher than the error for the density ($\text{err}_{\text{dens}} \approx 0.5\% \ldots 15\%$) and while an error of approximately 10% for

11

the RCE is acceptable, it would be too large for the density, rendering the parameter sets unusable for reproducing experimental results.

The loss function therefore needs to have different sensitivities in the two domains. To address this problem, the loss function value for every single property is projected to the closed interval $[0, 1]$, herein called non-linear projection (NLP), before being further processed in the loss function. The function z^* is used to convert the original loss function value z:

$$z^*(c, z) = 1 - e^{(-c \cdot z)} \tag{6}$$

The hyperparameter $c > 0$ controls the sensitivity of how z^* responds to changes in the loss function values z. For z the original loss function values of the different properties from equation (1) are used:

$$z_i^{\text{MM}}(x) = \left(\frac{f_i^{\text{QM}} - f_i^{\text{MM}}(x)}{f_i^{\text{QM}}} \right)^2 \ , \ z_j^{\text{MD}}(x) = \left(\frac{f_j^{\text{exp}} - f_j^{\text{MD}}(x)}{f_j^{\text{exp}}} \right)^2$$

Combining the NLP (see equation (6)) with the loss function $F(x)$ (see equation (1)) gives the resulting NLP loss function $F^*(x)$:

$$F^*(x) = \sum_{i=1}^{n} \omega_i^{\text{MM}} \left(z_i^{*,\text{MM}}(x) \right) + \sum_{j=1}^{m} \omega_j^{\text{MD}} \left(z_j^{*,\text{MD}}(x) \right) \tag{7}$$

2.3. Determining the Sensitivity Hyperparameter c

The hyperparameter c is used to control the sensitivity of the NLP loss function (see section 2.2). Since we already established that different domains need different loss sensitivity, how actual values for c can be obtained is shown in the following examples for the density and RCE.

In general, c needs to be adjusted such that an improvement in the simulation results yields a lower loss function value z^*, while a worsening would

12

yield a higher value (i.e. $\frac{\mathrm{d}}{\mathrm{d}z}z^*(c,z) \neq 0$). This is required because otherwise the gradient-based optimization algorithm can not calculate a descent direction to update the parameter set and suggest a better solution. Additionally, c must be chosen such that the loss function value for unwanted results does not fall below the threshold that causes the optimization to stop.

Analyzing various values for c with respect to the density, showed that $c_{\mathrm{density}} = 1000$ induce the aforementioned desired behavior. In figure 2 the loss function values, using the NLP loss function, for a hypothetical and unsuitable $c_{\mathrm{density}} = 10$ and a suitable $c_{\mathrm{density}} = 1000$ are shown (solid and dashed orange lines). The gray line shows the corresponding original loss function values (see equation (1)); Note, that those values can exceed 1, although this cannot be seen in the figure. Higher c_{density} values result in a narrower area where $z^* < 1$, and a steeper slope results in the transition areas. When c is too large, high loss function values can overlap with the range of acceptable errors (blue area), prohibiting the optimization algorithm from terminating. However, when c is too low, unwanted optimization results are assigned a low loss function value, erroneously causing the optimization to finish. For the optimization performed herein, the density sensitivity hyperparameter is set to $c_{\mathrm{density}} = 1000$. For that value, a well-balanced configuration between the aforementioned aspects is achieved.
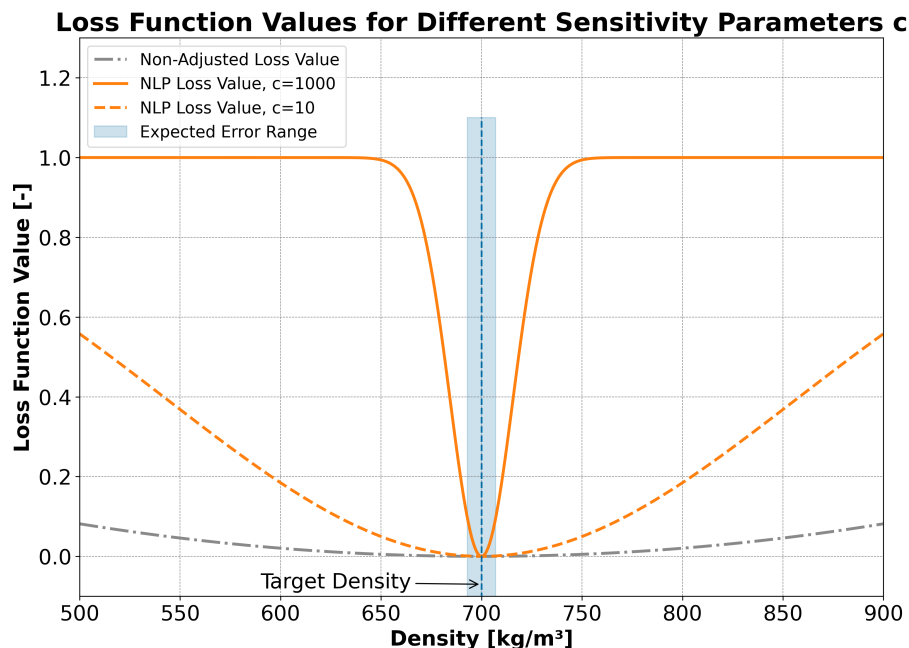
Loss Function Values for Different Sensitivity Parameters c

Figure 2: Impact of sensitivity hyperparameter c_{density} on the NLP loss function value (solid and dashed orange lines). The vertical blue line marks the target density and the blue area is the acceptable error for the optimization target (here: 1%). The original loss function value is visualized by the gray graph. Note, that the latter can exceed 1 (not shown in this figure).

The same scheme and rules need to be applied when determining c_{energy}. In figure 3 (subfigure (b)), it is shown that using $c_{\mathrm{energy}} = c_{\mathrm{density}} = 1000$ would result in the same loss function values for the RCE before and for an intermediate iteration of the optimization (black and gray lines, respectively). This is a problem because when the loss function value of a given parameter set $F(x)$ (e.g. the loss function values for the initial RCE; black graph) is the same as or very similar to another value $F(x + h)$ (e.g. the loss function

14

values for the RCE of an intermediate iteration of the optimization, when the force field parameters x are changed by a small amount h; gray graph), the resulting gradient $\nabla F(x) = 0$ and no descent direction can be recognized. Analyzing various values for c with respect to the RCE showed that by choosing $c_{energy} = 1$, the aforementioned problem does not occur and yields the desired behavior regarding the reproduced RCE and loss function values (see figure 3, subfigures (a) and (c), respectively).

15

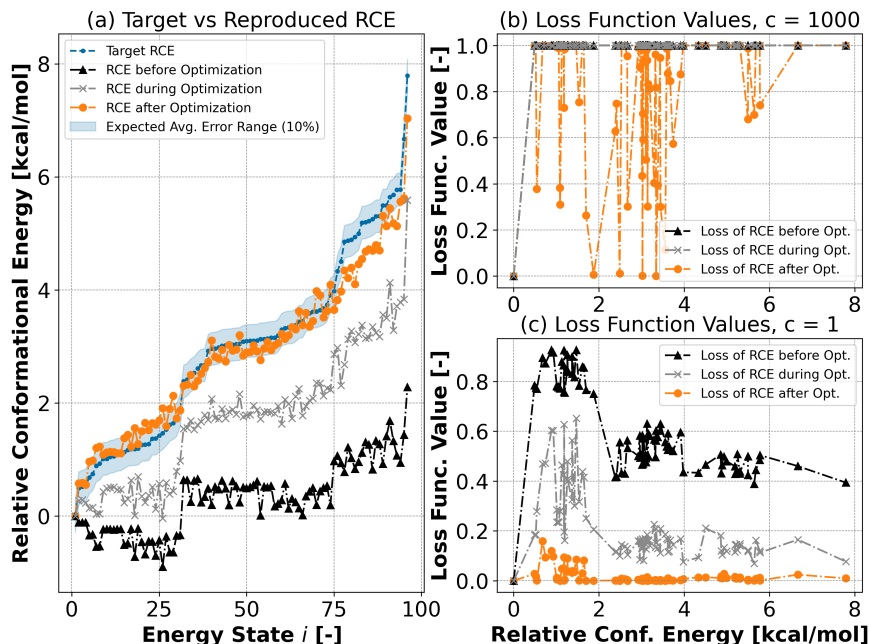**Loss Function Values for Different Sensitivity Parameters c**

Figure 3: Subfigure (a): the reproduced RCE before (black graph), for an intermediate iteration of the optimization (gray graph) and after (orange graph) the optimization compared to their target values (blue graph), including an 10% error range (blue area).

Subfigure (b): Loss function values corresponding to the RCE before, for an intermediate iteration of the optimization and after the optimization (black, gray and orange graphs, respectively) for $c_{\text{energy}} = 1000$. Note, that the gray and black graphs overlap.

Subfigure (c): Loss function values corresponding to the RCE before, for an intermediate iteration of the optimization and after the optimization (black, gray and orange graphs, respectively) for $c_{\text{energy}} = 1$.

2.4. Simulation Tools and Setup

The optimization workflow used herein is called Force FieLd Optimization Workflow (FFLOW), which is a modular optimization toolbox containing structures and methods introduced by Gradient-based Optimization

16

Workflow (GROW)[21]. The FFLOW software files, scripts for parameter conversion (Gromacs to Amber), steering scrips that manage, for example, the queuing system, used input files, and all simulation configurations are available on GitHub via [22]. The density calculations were carried out using Gromacs [23, 24], while the RCE were computed by Amber [2].

The following fourteen inter-domain weight distribution setups are investigated, each applied to the four intra-domain balancing approaches: "0-100", "05-95", "10-90", "15-85", "20-80", "25-75", "40-60", "50-50", "60-40", "80-20", "85-15", "90-10", "95-05" and "100-0". For all of those (i.e., $14 \cdot 4$) setups two different loss functions are studied, the original and the NLP loss function (see section 2.2). In total, 112 (i.e., $14 \cdot 4 \cdot 2$) different setups are investigated.

Note, that the MM calculations for reproducing the RCE are deterministic, and for the MD simulations of the density, equilibrated systems are used that were initialized with the identical "random" seeds. Thus, all calculation results have a very low variance, as shown in previous work [18], and thus are not statistically repeated or analyzed.

3. Results

In this section, the results for the original loss function (equation (1)), followed by the results using the NLP loss function (equation (7)) are presented, including every combination of inter- and intra-domain balancing used. Finally, the best overall optimized parameter set is presented.

17

3.1. Original Loss Function

The errors of the optimization objectives (i.e. density and RCE) using the original loss function (equation (1)) are visualized in figure 4. The errors for the density (blue line) and RCE (orange line) are shown depending on the overall weight that is assigned to the density weighting factor (i.e. the inter-domain balancing). Consequently, an x-axis value of 20% stands for the "20-80" balancing where 80% of the total weight is distributed among the RCE weighting factors and 20% is assigned to the density weighting factor. The subfigures show the data for the four different intra-domain weighting factor balancing strategies.

18

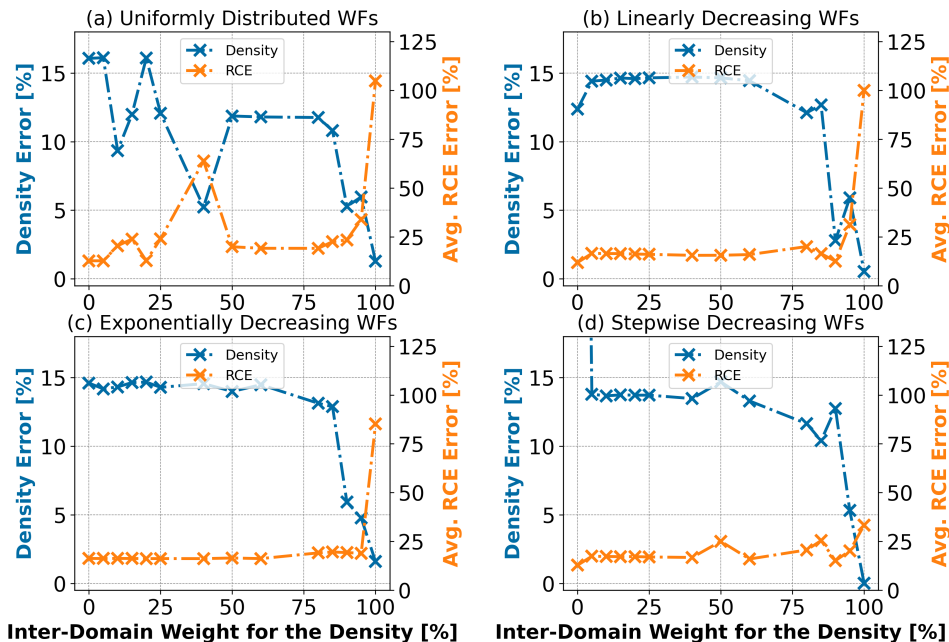**Errors of Reproduced Density and RCE using the Original Loss Function**

Figure 4: Errors for the reproduction of the density (blue) and RCE (orange). The FF-PARAMS optimizations are performed using the original loss function and all combinations of inter- and intra-domain weighting factor balancing approaches (figures (a) – (d)).

For every setup, the density and RCE error curves intersect in the region where approximately 95% to 99% of the weight is assigned to the density. The location of the intersection is an interesting characteristic because it is an indicator for a well-balanced weighting factor distribution. Note that this does not necessarily correspond to the lowest combined error (i.e. the sum of the density and RCE errors). The intersections around "40-60" in figure 4(a) are caused by the optimization algorithm being stuck in a local minimum, which is a general problem for local optimization algorithms. The corresponding resulting parameter set also differs from the other resulting pa-

19

rameter sets (see tables 2, 3, 4 and 5 in section *Supplementary Information*). Generally, the resulting parameter sets do not show a clearly favorable parameter combination (see figure 5). Some combinations of the force field parameters σ_H, ϵ_C and partially σ_C occur more frequently than others, but other combinations can result in similar or even lower loss function values.

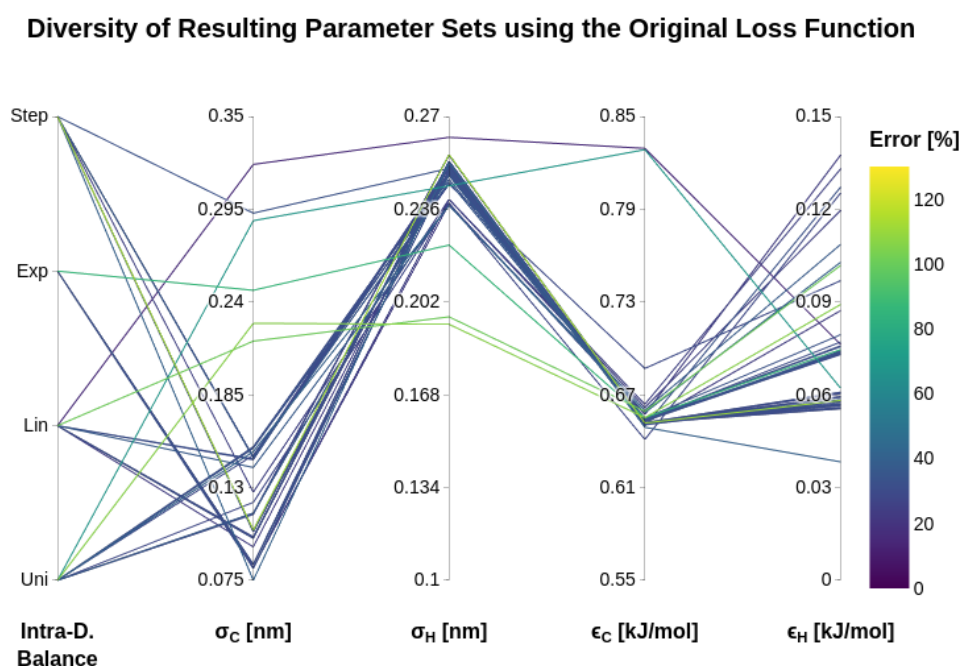Figure 5: Resulting Lennard-Jones parameters (i.e. 56 optimized parameter sets) using the original loss function and all combinations of inter- and intra-domain balancing approaches.

3.2. NLP Loss Function

Optimizing the Lennard-Jones parameters using the NLP loss function (equation (7)) shifts the intersection points of the graphs to a balancing where approximately 25% to 30% of the overall weight is assigned to the

20

density weighting factor (see figure 6). All resulting parameter sets and their corresponding errors are listed in tables 6, 7, 8 and 9 in section *Supplementary Information*.

Errors of Reproduced Density and RCE using the NLP Loss Function
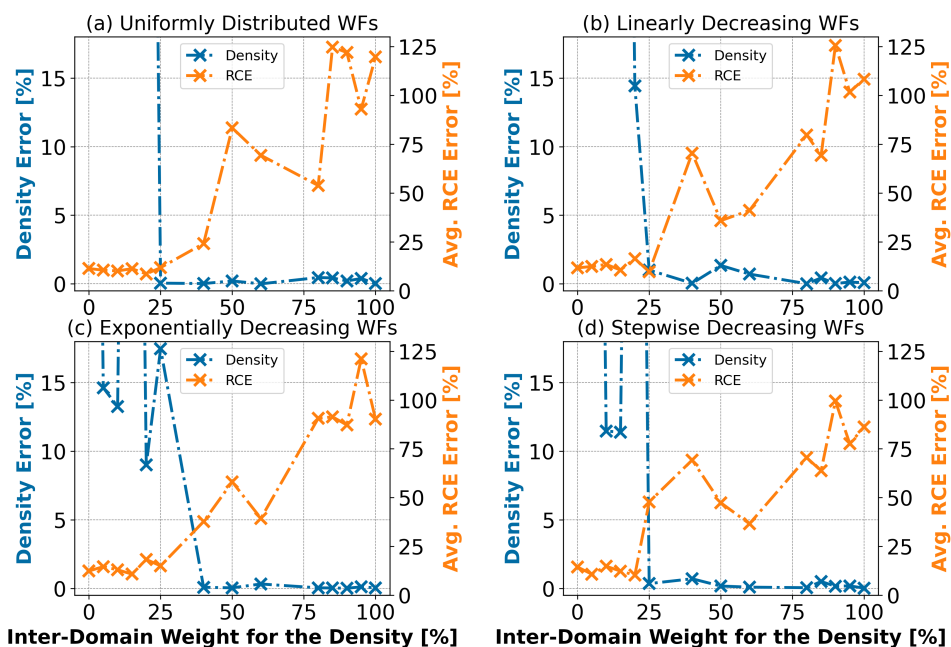
Figure 6: Errors for the reproduction of the density (blue) and RCE (orange). The FFPARAMS optimizations are performed using the NLP loss function and all combinations of inter- and intra-domain weighting factor balancing approaches (figures (a) – (d)).

On average, the combined errors (i.e. the sum of the density and RCE errors) using the NLP loss function are higher than the combined errors using the original loss function. However, the optimizations resulting in the lowest combined error are predominately achieved when applying the NLP to the loss function (see figure 7).

21

Combined Errors of Reproduced Density and RCE
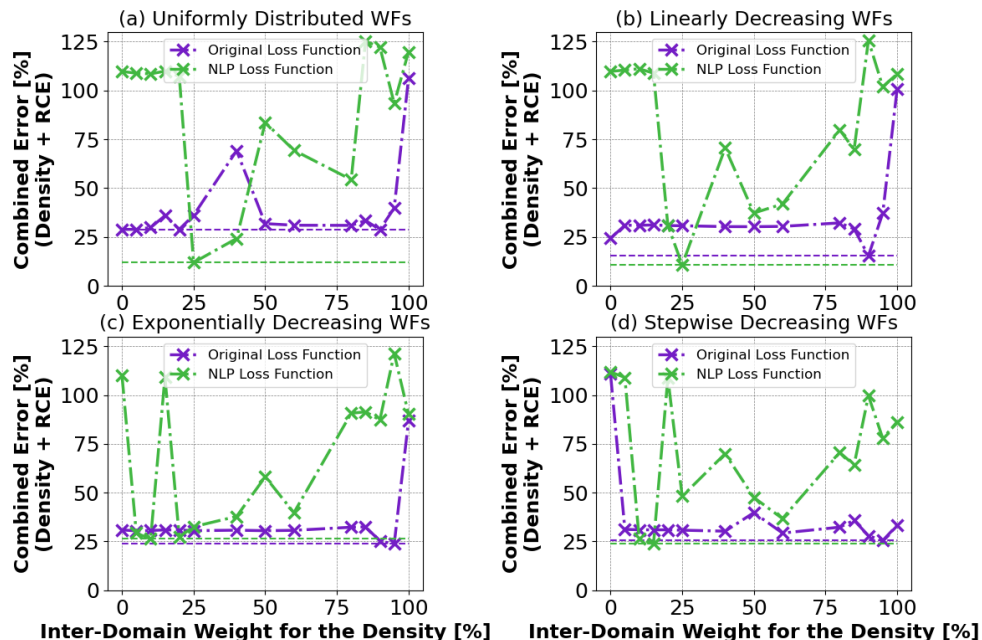
Figure 7: Comparison of the combined errors using the original loss function (purple) and the NLP loss function (green). All combinations of inter- (on the x-axis) and intra-domain (figures (a) – (d)) weighting factor balancing approaches are used. The lowest combined errors for the setups using the original and NLP loss function are marked with a horizontal dashed line.

Similar to the resulting parameters using the original loss function, there is an even larger diversity of the optimization results (see figure 8). This is more evidence that the loss landscape is highly multi-modal and gradient-based optimization can get stuck in wildly different local optima even depending on the weighting strategy in the loss function.

22
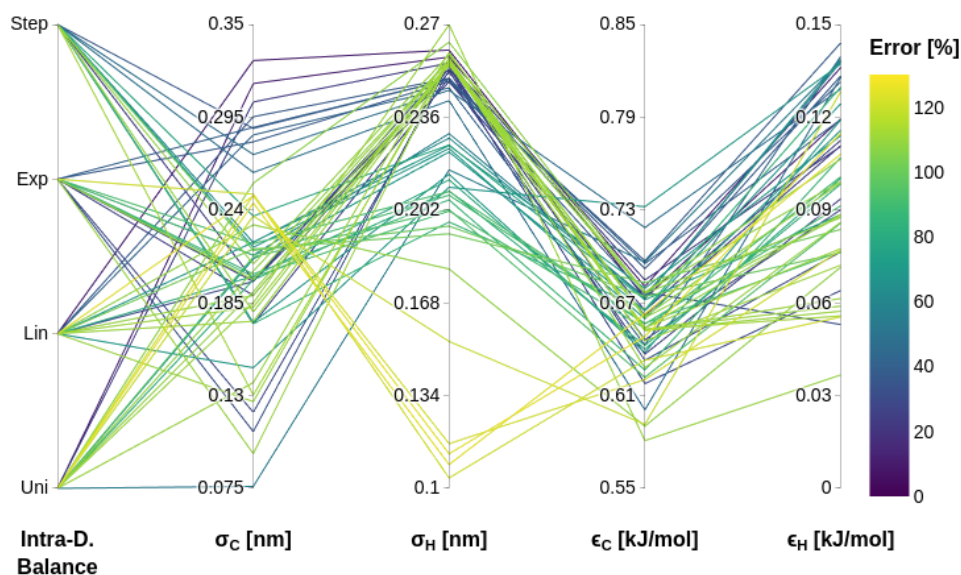
Figure 8: Resulting Lennard-Jones Parameters (i.e. 56 optimized parameter sets) using the NLP loss function and all combinations of inter- and intra-domain balancing approaches.

3.3. Best Optimized Parameter Set

The best overall result for the combined error of density and RCE yields the optimization using the NLP loss function, linearly decreasing WFs for the RCE and an overall balancing between density and RCE WFs of 25% to 75% (i.e. the "25-75" setup), respectively. The resulting FFParams and their corresponding errors, err_{dens} for the density and err_{ener} for the RCE, is shown in table 1.

Table 1: Resulting optimized parameter set with the lowest combined error. The setup optimization used for this result combines the NLP loss function, linearly decreasing WFs for the RCE and an inter-domain balancing of 25% for the density and 75% for the RCE.

σ_C [nm]	σ_H [nm]	ϵ_C [kJ/mol]	ϵ_H [kJ/mol]	err_{dens}	err_{ener}
0.3286	0.2606	0.6730	0.1194	1.0 %	9.75 %

The reproduced density is $(707.0 \pm 4.7)\frac{\text{kg}}{\text{m}^3}$, leading to an error of $1.0\,\% \pm 0.67\,\%$. For the herein used target density of $0.7\,\frac{\text{g}}{\text{cm}^3}$ [20], that is converted to $700\,\frac{\text{kg}}{\text{m}^3}$, no error range is provided in the data's source [25]. However, other literature, for example the Chemistry Webbook [26] of the National Institute of Standards and Technology (NIST), report an estimated error of $0.1\,\%$ to $0.3\,\%$ for their density values [27, 28]. Therefore, the herein used target density is assumed to have an error less or equal to $0.3\,\%$.

The average error of the RCE is $9.75\,\%$ (for the individual RCE values see table 10 and figure 9 in section *Supplementary Information*). The average error for the RCE is calculated by adding all individual errors and dividing the sum by the amount of RCE. If the (absolute) error for the target RCE based on MP2.5/AVTZ's reproduction of CCSD(T) results (Table 2 of reference [19]) is estimated, the upper limit was $-0.012\,\text{kcal}\cdot\text{mol}^{-1}$ as computed for *n*-hexane (i.e., 12 conformers). This results in an average relative error of $-0.91\,\%$ and the herein achieved results and error ranges are not as good as those results and error ranges. However, considering the different theories (i.e. MM vs. CCSD(T) or MP2.5/AVTZ calculations) and the required time to compute the results, the average relative error range of $9.75\,\%$ achieved herein is acceptable. It is worth noting that this level of error is similar when

24

comparing 96 Density Functional Theory (DFT) (B2K-PLYP-D) computed octane values to MP2.5/AVTZ values, which has an error of $+0.19$kcal$\cdot$mol^{-1} (i.e., $9.43\,\%$) [19].

In total, the previously achieved results [18] are improved. The average error of the RCE increased from $7.85\,\%$ to $9.75\,\%$, but the error for the density is decreased substantially from $-4.14\,\% \pm 0.04\,\%$ to $1\,\% \pm 0.67\,\%$.

4. Discussion

For the original loss function, the graphs in figure 4 show that the most balanced inter-domain weighting factor distribution is reached when most of the weight ($\sim 95\,\%$) is assigned to the density. However, for this setup, the errors for the density reproduction are large with the best values lying between $2.80\,\%$ to $5.90\,\%$ (see tables 2, 3, 4 and 5 in section *Supplementary Information*). Further analyses of the loss function suggest that applying a non-linear projection (NLP) to the individual parts of the loss function is beneficial, increasing the comparability of the particular optimization objectives. The NLP ensures that the loss function values for the particular objectives have the same order of magnitude, once the sensitivity hyperparameter c is configured appropriately.

Using the NLP loss function shifts the most balanced inter-domain weighting factor distribution to a setup with $\sim 25\,\%$ of the overall weight assigned to the density (see figures 6 and 7 as well as tables 6, 7, 8 and 9 in section *Supplementary Information*). The NLP works as expected and improves the comparability of the errors (i.e. the loss function values) of the different target property domains. Furthermore, the best optimization result is achieved

25

by using the NLP loss function. However, this method introduces an additional layer of complexity represented by the sensitivity hyperparameter c. It needs to be determined and configured for every optimization objective separately and requires a deeper insight into that specific optimization objective. This might not be a problem for experienced users but is oppositional to a user-friendly, fast and automatized force field optimization workflow.

The diversity of the optimization results (see figures 5 and 8) shows the multi-modal nature of the loss function's landscape. Almost every optimization run results in a different FFPARAMS set, depending on the optimization setup. A major disadvantage of this local optimization algorithm is that it can get stuck in a local minimum of the optimization landscape, unable to discover other minima that might be representatives of more suitable parameter sets. A consequence is that the current optimization workflow is very dependent on the initial parameter set. This might be a small issue when an already well-performing force field is re-optimized, but can be challenging for newly investigated models of molecules.

5. Conclusion

This study's goal is to reduce the reproduction error of the density, arisen in a previous study [18], while maintaining the accuracy of the RCE reproduction. This goal is accomplished by adapting the particular WFs and the objective function used for this multiscale optimization process. The error for the density reproduction is decreased by a considerable amount, while the error for the reproduction of the RCE remains at approximately the same level.

26

Compared to the previously achieved results, the error regarding the bulk-phase density is improved from $(-4.14 \pm 0.04)\,\%$ to $(1.0 \pm 0.67)\,\%$, which is an acceptable error considering experimental uncertainties of $0.1\,\%$ to $0.3\,\%$, keeping in mind that MD and MM calculations are mathematical models based on several assumptions and simplifications. The average error for the RCE reproduction, however, slightly increased from $7.85\,\%$ to $9.75\,\%$. This is still approximately the same quality of results. This error range is not as good as the target data's average error of $-0.91\,\%$, however, considering the necessary time to compute the RCE using the different modeling theories, an average relative error of $9.75\,\%$ is acceptable, especially compared to their average reproduction error of $\sim 100\,\%$ prior to the multiscale optimization, this is a substantial improvement. It is also worth noting that this error level is similar to that seen when comparing DFT (B2K-PLYP-D) to MP2.5/ATZ computed values.

To tackle the challenge of the loss function's multi-modality and diversity of optimization results for future development in automated custom force field parameter optimization, we propose to use a global optimization approach. Additionally, the current optimization scheme yields a single resulting parameter set. However, the different optimization setups show that there are different parameter sets that might be promising, depending on the intended use case. Furthermore, the two optimization objectives used herein seem to be contrary to one another because, if there is an improvement for one property, often the error of the other increases. Thus, for further development, we additionally plan to use a multi-objective optimization with multiple solutions.

27

Acknowledgment

AUTHOR INFORMATION

Corresponding Author

Dirk Reith, Department of Engineering and Communication (DEC), Bonn-Rhein-Sieg University of Applied Sciences, Sankt Augustin, Germany; Orcid orcid.org/0000-0003-1480-6745; Email: dirk.reith@h-brs.de

Authors

Robin Strickstrock, Department of Engineering and Communication (DEC), Bonn-Rhein-Sieg University of Applied Sciences, Sankt Augustin, Germany; Orcid orcid.org/0000-0002-5092-3677

Alexander Hagg, Department of Computer Science (CS), Bonn-Rhein-Sieg University of Applied Sciences, Sankt Augustin, Germany; Orcid: orcid.org/0000-0002-8668-1796

Marco Hülsmann, Department of Computer Science, Bonn-Rhein-Sieg University of Applied Sciences, Sankt Augustin, Germany; Orcid: orcid.org/0000-0003-3918-7792

Karl N. Kirschner, Department of Computer Science(CS), Bonn-Rhein-Sieg University of Applied Sciences, Sankt Augustin, Germany; Orcid: orcid.org/0000-0002-4581-920X

Author Contributions

The author contributions follow the CRediT taxonomy (https://casrai.org/credit). **RS's** contributions included conceptualization, data curation, formal analysis, investigation, methodology, project administration, software, validation, visualization, writing - original draft and writing - review & editing.

AH's contributions included formal analysis, visualization and writing - review & editing.

MH's contributions included formal analysis and writing - review & editing.

KNK's contributions included conceptualization, funding acquisition, resources, supervision, visualization, and writing - review & editing.

DR's contributions included conceptualization, funding acquisition, resources, supervision, visualization, and writing - review & editing.

Declaration of Interests

The authors declare that they have no known competing financial interests or personal relationships that could have appeared to influence the work reported in this paper. All authors have given approval to the manuscript's final version.

Supplementary Information

Data and Software Availability

The code and input data used to perform the optimizations herein are available at: `https://github.com/rstrickstrock/tuning_weighting-factors_objective-function.git`

Note: The code is provided for reproduction purposes and may need to be adapted to the IT infrastructure it is used on.

The MP2.5/AVTZ optimized geometries for octane are available within the SI material of reference [19].

30

Results using the Original Loss Function

Table 2: Results of the parameter optimization using the original loss function (see equation (1)) and the Uniformly Distributed WFs approach. The Errors err_ρ, err_{RCE} and err_{comb}, for the density, RCE and their sum, respectively, are given in [%]. The units of σ and ϵ are [nm] and [kJ/mol], respectively.

Inter-dom. Balance	Uniformly Distributed WFs						
	σ_{C}	σ_{H}	ϵ_{C}	ϵ_{H}	err_ρ	err_{RCE}	err_{comb}
0-100	0.11485	0.25605	0.65199	0.05944	16.07	12.76	28.83
05-95	0.11411	0.25581	0.6519	0.06037	16.12	12.74	28.86
10-90	0.14924	0.24515	0.68702	0.09691	9.35	20.45	29.80
15-85	0.11487	0.24838	0.65201	0.05845	11.98	23.87	35.85
20-80	0.11422	0.2557	0.65204	0.06058	16.10	12.77	28.87
25-75	0.11472	0.24833	0.652	0.05825	12.06	24.02	36.08
40-60	0.28822	0.24456	0.82853	0.06211	5.24	63.90	69.14
50-50	0.15399	0.24914	0.65446	0.07556	11.87	19.93	31.80
60-40	0.15417	0.24953	0.65405	0.07587	11.80	19.16	30.96
80-20	0.15339	0.24925	0.65378	0.07709	11.76	19.13	30.89
85-15	0.15335	0.24696	0.65488	0.07945	10.80	22.57	33.37
90-10	0.12123	0.23834	0.64111	0.12527	5.28	23.47	28.75
95-05	0.15132	0.23737	0.65843	0.10286	5.97	33.81	39.78
100-0	0.22736	0.19383	0.6552	0.08922	1.28	104.88	106.16

31

Table 3: Results of the parameter optimization using the original loss function (see equation (1)) and the Linearly Decreasing WFs approach. The Errors err_ρ, err_{RCE} and err_{comb}, for the density, RCE and their sum, respectively, are given in [%]. The units of σ and ϵ are [nm] and [kJ/mol], respectively.

Inter-dom. Balance	Linearly Decreasing WFs						
	σ_C	σ_H	ϵ_C	ϵ_H	err_ρ	err_{RCE}	err_{comb}
0-100	0.09485	0.2506	0.65142	0.08723	12.38	11.86	24.24
05-95	0.09996	0.25296	0.65158	0.05653	14.41	16.53	30.94
10-90	0.09999	0.25301	0.65153	0.05653	14.49	16.47	30.96
15-85	0.10005	0.25301	0.65159	0.0566	14.64	16.44	31.08
20-80	0.1001	0.25319	0.65159	0.0566	14.59	16.22	30.81
25-75	0.1002	0.2533	0.65153	0.05663	14.65	16.06	30.72
40-60	0.10048	0.25368	0.65152	0.05679	14.71	15.55	30.26
50-50	0.10066	0.25359	0.65132	0.05701	14.65	15.58	30.23
60-40	0.10078	0.25326	0.65104	0.05715	14.44	15.94	30.38
80-20	0.147	0.24902	0.65467	0.07322	12.11	20.05	32.16
85-15	0.14656	0.25109	0.653	0.07359	12.67	16.42	29.09
90-10	0.32156	0.26236	0.82934	0.07625	**2.80**	**12.52**	**15.32**
95-05	0.14191	0.23737	0.66014	0.10862	5.90	31.23	37.13
100-0	0.2168	0.19657	0.65935	0.10183	0.53	100.08	100.61

32

Table 4: Results of the parameter optimization using the original loss function (see equation (1)) and the Exponentially Decreasing WFs approach. The Errors err_ρ, err_{RCE} and err_{comb}, for the density, RCE and their sum, respectively, are given in [%]. The units of σ and ϵ are [nm] and [kJ/mol], respectively.

Inter-dom. Balance	Exponentially Decreasing WFs						
	σ_C	σ_H	ϵ_C	ϵ_H	err_ρ	err_{RCE}	err_{comb}
0-100	0.08436	0.25299	0.65191	0.05556	14.60	16.28	30.88
05-95	0.08435	0.25301	0.65191	0.05555	14.18	16.25	30.43
10-90	0.08434	0.25301	0.6518	0.05551	14.32	16.28	30.60
15-85	0.08439	0.25302	0.65179	0.05551	14.64	16.27	30.91
20-80	0.08448	0.25302	0.65199	0.05564	14.67	16.20	30.87
25-75	0.08447	0.25304	0.65193	0.05555	14.29	16.22	30.51
40-60	0.08444	0.25302	0.65208	0.05567	14.56	16.20	30.76
50-50	0.08427	0.25279	0.65196	0.05563	13.99	16.51	30.50
60-40	0.0845	0.25293	0.65137	0.05596	14.48	16.21	30.69
80-20	0.08198	0.25043	0.65151	0.05717	13.13	19.13	32.26
85-15	0.08423	0.25	0.65054	0.05793	12.88	19.59	32.47
90-10	0.08252	0.23958	0.66181	0.11964	5.93	19.30	25.23
95-05	0.0826	0.23798	0.65725	0.13754	4.77	18.92	23.69
100-0	0.24694	0.22287	0.65516	0.07463	1.59	85.16	86.75

Table 5: Results of the parameter optimization using the original loss function (see equation (1)) and the Stepwise Decreasing WFs approach. The Errors err_ρ, err_{RCE} and err_{comb}, for the density, RCE and their sum, respectively, are given in [%]. The units of σ and ϵ are [nm] and [kJ/mol], respectively.

Inter-dom. Balance	Stepwise Decreasing WFs						
	σ_{C}	σ_{H}	ϵ_{C}	ϵ_{H}	err_ρ	err_{RCE}	err_{comb}
0-100	0.1048	0.25603	0.6517	0.05818	97.94	12.83	110.77
05-95	0.10482	0.25216	0.65172	0.05769	13.79	17.40	31.19
10-90	0.1045	0.2518	0.65171	0.05921	13.67	17.30	30.97
15-85	0.10451	0.25188	0.65215	0.05924	13.74	17.19	30.93
20-80	0.10452	0.25184	0.6517	0.05927	13.72	17.23	30.95
25-75	0.10367	0.25156	0.65177	0.06075	13.72	17.04	30.76
40-60	0.10408	0.25172	0.65184	0.06085	13.47	16.79	30.26
50-50	0.07504	0.25308	0.64896	0.03831	14.69	25.04	39.73
60-40	0.14765	0.25156	0.65368	0.07301	13.30	16.00	29.30
80-20	0.14756	0.2487	0.65298	0.07324	11.64	20.66	32.30
85-15	0.14793	0.24602	0.65397	0.0739	10.40	25.43	35.83
90-10	0.1483	0.25191	0.65293	0.07419	12.75	15.19	27.94
95-05	0.12727	0.23966	0.66385	0.13306	5.33	20.14	25.47
100-0	0.29268	0.25098	0.64966	0.12716	0.02	33.29	33.31

34

Results using the NLP *Loss Function*

Table 6: Results of the parameter optimization using the NLP loss function (see equation (7)) and the Uniformly Distributed WFs approach. The Errors err_ρ, err_{RCE} and err_{comb}, for the density, RCE and their sum, respectively, are given in [%]. The units of σ and ϵ are [nm] and [kJ/mol], respectively.

Inter-dom. Balance	Uniformly Distributed WFs						
	σ_{C}	σ_{H}	ϵ_{C}	ϵ_{H}	err_ρ	err_{RCE}	err_{comb}
0-100	0.13767	0.25982	0.65293	0.05891	98.37	11.36	109.73
05-95	0.19152	0.25709	0.66034	0.08798	98.37	10.49	108.86
10-90	0.20372	0.25708	0.66132	0.09876	98.38	10.13	108.51
15-85	0.1849	0.26988	0.58088	0.03665	98.62	11.28	109.90
20-80	0.2559	0.2635	0.67679	0.10644	98.65	8.59	107.24
25-75	0.31496	0.25805	0.68059	0.13604	0.05	11.81	11.86
40-60	0.30405	0.25587	0.68475	0.11057	0.02	24.15	24.17
50-50	0.19861	0.20899	0.64243	0.09839	0.21	83.39	83.60
60-40	0.21098	0.22327	0.66489	0.12433	0.00	69.36	69.36
80-20	0.07612	0.21672	0.69629	0.13827	0.46	53.87	54.33
85-15	0.24418	0.10871	0.66282	0.10805	0.43	124.79	125.22
90-10	0.24885	0.11637	0.62035	0.07704	0.21	122.01	122.22
95-05	0.21218	0.20217	0.62182	0.08574	0.39	93.02	93.41
100-0	0.23644	0.15383	0.59135	0.12819	0.02	119.81	119.83

35

Table 7: Results of the parameter optimization using the NLP loss function (see equation (7)) and the Linearly Decreasing WFs approach. The Errors err_ρ, err_{RCE} and err_{comb}, for the density, RCE and their sum, respectively, are given in [%]. The units of σ and ϵ are [nm] and [kJ/mol], respectively.

Inter-dom. Balance	Linearly Decreasing WFs						
	σ_{C}	σ_{H}	ϵ_{C}	ϵ_{H}	err_ρ	err_{RCE}	err_{comb}
0-100	0.12641	0.25769	0.65243	0.06138	98.07	11.69	109.76
05-95	0.17404	0.25525	0.65386	0.0775	98.03	12.42	110.45
10-90	0.18246	0.25613	0.64534	0.07214	97.66	13.48	111.14
15-85	0.1893	0.25491	0.67685	0.09918	98.25	10.63	108.88
20-80	0.19764	0.25485	0.63278	0.07647	14.42	16.50	30.92
25-75	0.3286	0.2606	0.67297	0.11941	**1.00**	**9.75**	**10.75**
40-60	0.22094	0.22559	0.67936	0.11403	0.04	70.56	70.60
50-50	0.29529	0.25021	0.6922	0.13141	1.34	35.95	37.29
60-40	0.28451	0.24679	0.64267	0.13965	0.71	41.20	41.91
80-20	0.20069	0.21308	0.63993	0.10021	0.01	79.90	79.91
85-15	0.14655	0.21033	0.73213	0.13719	0.43	69.40	69.83
90-10	0.24833	0.11266	0.64822	0.11476	0.02	125.78	125.80
95-05	0.2168	0.1933	0.68302	0.08373	0.13	101.92	102.05
100-0	0.23122	0.18039	0.59022	0.07149	0.08	108.52	108.60

36

Table 8: Results of the parameter optimization using the NLP loss function (see equation (7)) and the Exponentially Decreasing WFs approach. The Errors err_ρ, err_{RCE} and err_{comb}, for the density, RCE and their sum, respectively, are given in [%]. The units of σ and ϵ are [nm] and [kJ/mol], respectively.

Inter-dom. Balance	Exponentially Decreasing WFs						
	σ_{C}	σ_{H}	ϵ_{C}	ϵ_{H}	err_ρ	err_{RCE}	err_{comb}
0-100	0.09552	0.25671	0.65192	0.05728	97.72	12.42	110.14
05-95	0.12007	0.25315	0.61773	0.06398	14.62	14.65	29.27
10-90	0.18941	0.25381	0.64604	0.09007	13.25	13.02	26.27
15-85	0.19869	0.25722	0.62799	0.08599	98.41	10.82	109.23
20-80	0.19765	0.24898	0.66514	0.11251	9.01	18.30	27.31
25-75	0.10862	0.2556	0.67672	0.053	17.47	15.06	32.53
40-60	0.28039	0.24916	0.69717	0.144	0.08	37.73	37.81
50-50	0.21316	0.23	0.67354	0.13784	0.04	58.06	58.10
60-40	0.28895	0.24989	0.69536	0.11924	0.32	39.38	39.70
80-20	0.20033	0.20162	0.65347	0.10073	0.04	90.60	90.64
85-15	0.22003	0.20879	0.65677	0.07661	0.03	91.38	91.41
90-10	0.20204	0.20572	0.62651	0.10699	0.01	87.20	87.21
95-05	0.2494	0.10379	0.63284	0.05545	0.11	121.15	121.26
100-0	0.21329	0.20744	0.65638	0.09134	0.04	90.18	90.22

37

Table 9: Results of the parameter optimization using the NLP loss function (see equation (7)) and the Stepwise Decreasing WFs approach. The Errors err_ρ, err_{RCE} and err_{comb}, for the density, RCE and their sum, respectively, are given in [%]. The units of σ and ϵ are [nm] and [kJ/mol], respectively.

Inter-dom. Balance	Stepwise Decreasing WFs						
	σ_C	σ_H	ϵ_C	ϵ_H	err_ρ	err_{RCE}	err_{comb}
0-100	0.13033	0.25609	0.65261	0.05574	97.33	14.44	111.76
05-95	0.17957	0.25568	0.65359	0.0886	98.20	10.80	109.00
10-90	0.17252	0.25047	0.63676	0.0936	11.47	14.85	26.32
15-85	0.19862	0.25244	0.66197	0.11078	11.38	12.36	23.74
20-80	0.20799	0.25884	0.67612	0.08752	98.45	10.29	108.74
25-75	0.26226	0.24207	0.60066	0.13286	0.35	47.80	48.15
40-60	0.17351	0.2151	0.63783	0.11913	0.70	69.25	69.95
50-50	0.27288	0.24587	0.71864	0.12912	0.17	47.36	47.53
60-40	0.28839	0.24985	0.6747	0.13335	0.09	36.62	36.71
80-20	0.21791	0.22452	0.65969	0.11574	0.05	70.47	70.52
85-15	0.22073	0.22837	0.67301	0.1388	0.50	63.72	64.22
90-10	0.21606	0.19612	0.67408	0.07617	0.16	99.47	99.63
95-05	0.23638	0.22583	0.67193	0.08854	0.18	77.60	77.78
100-0	0.17262	0.19763	0.66564	0.12969	0.02	86.23	86.25

38

5.1. Relative Conformational Energies

Table 10: Target and reproduced RCE. The RCE calculations are performed using the best optimized parameter set (see section 3.3). The units of the RCE are given in kcal/mol

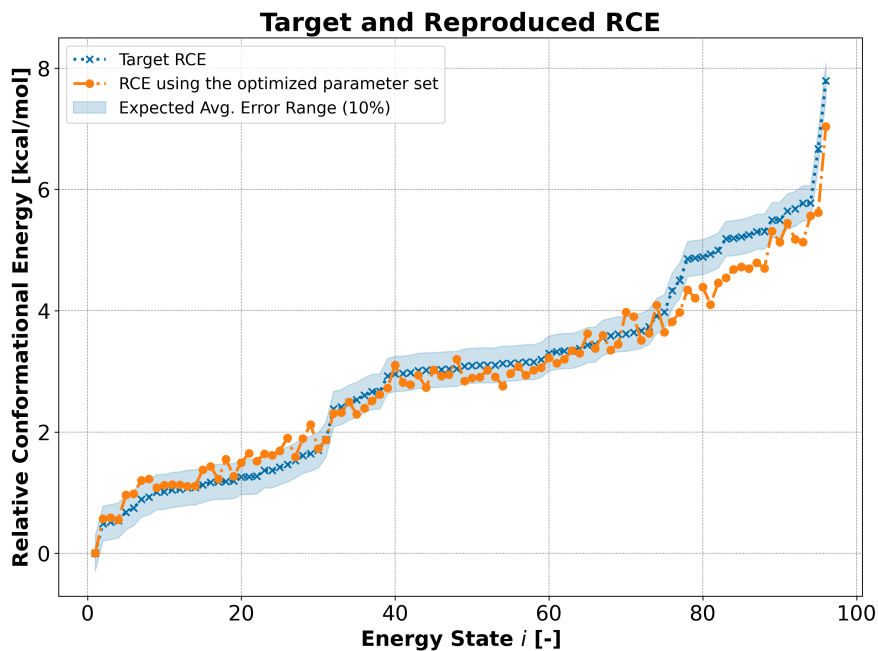|	Target	Reprod.		Target	Reprod.		Target	Reprod.
conf-1	0	0	conf-33	1.876	1.87128	conf-65	3.102	2.91168
conf-2	0.491	0.57358	conf-34	3.011	2.93908	conf-66	4.854	4.34558
conf-3	0.746	0.98098	conf-35	3.129	2.75948	conf-67	5.496	5.31028
conf-4	0.542	0.55378	conf-36	2.963	2.81948	conf-68	5.188	4.54538
conf-5	1.195	1.27148	conf-37	3.588	3.35228	conf-69	5.496	5.13038
conf-6	1.17	1.43488	conf-38	3.323	3.13338	conf-70	4.887	4.39058
conf-7	1.057	1.12778	conf-39	3.093	2.89368	conf-71	4.934	4.10358
conf-8	1.183	1.55428	conf-40	3.101	2.90358	conf-72	5.681	5.17998
conf-9	1.084	1.10778	conf-41	2.959	3.10358	conf-73	3.141	3.08148
conf-10	1.261	1.64818	conf-42	3.153	3.01958	conf-74	5.304	4.79238
conf-11	1.089	1.10998	conf-43	3.193	3.06208	conf-75	4.871	4.20938
conf-12	0.679	0.96138	conf-44	1.466	1.90368	conf-76	0.518	0.58738
conf-13	1.27	1.52108	conf-45	3.375	3.29948	conf-77	1.012	1.12528
conf-14	0.929	1.22548	conf-46	3.443	3.37788	conf-78	2.98	2.78138
conf-15	1.257	1.49848	conf-47	2.531	2.29248	conf-79	3.083	2.83908
conf-16	1.128	1.37668	conf-48	3.021	3.02498	conf-80	3.129	2.96508
conf-17	1.047	1.13348	conf-49	2.664	2.51618	conf-81	3.031	2.92508
conf-18	1.37	1.61768	conf-50	2.487	2.49558	conf-82	3.043	3.19938
conf-19	1.368	1.64128	conf-51	1.644	2.12518	conf-83	3.643	3.90308
conf-20	1.181	1.22368	conf-52	3.614	3.44808	conf-84	3.436	3.62168
conf-21	0.888	1.20438	conf-53	3.736	3.62678	conf-85	3.915	4.09338
conf-22	2.381	2.30608	conf-54	3.296	3.22098	conf-86	4.501	3.97408
conf-23	1.011	1.08218	conf-55	3.101	3.01878	conf-87	3.977	3.64588
conf-24	1.421	1.69198	conf-56	3.34	3.34238	conf-88	5.306	4.69928
conf-25	1.611	1.89278	conf-57	3.018	2.73408	conf-89	5.219	4.72068
conf-26	1.699	1.72868	conf-58	4.33	3.81988	conf-90	5.197	4.68178
conf-27	2.412	2.32238	conf-59	3.619	3.97668	conf-91	5.25	4.69288
conf-28	2.669	2.61838	conf-60	3.555	3.59408	conf-92	5.777	5.56458
conf-29	1.531	1.58828	conf-61	3.337	3.19948	conf-93	5.772	5.13098
conf-30	2.608	2.39378	conf-62	4.995	4.45968	conf-94	6.667	5.62108
conf-31	3.153	2.93728	conf-63	3.039	2.94798	conf-95	5.641	5.44538
conf-32	2.923	2.72408	conf-64	3.671	3.51228	conf-96	7.791	7.03588

39

Figure 9: Table 10 visualized. Target and reproduced RCE. The RCE calculations are performed using the best optimized parameter set (see section 3.3).

References

[1] J. Wang, R. M. Wolf, J. W. Caldwell, P. A. Kollman, D. A. Case, Development and testing of a general amber force field, Journal of Computational Chemistry 25 (9) (2004) 1157–1174. doi:https://doi.org/10.1002/jcc.20035.
URL   https://onlinelibrary.wiley.com/doi/abs/10.1002/jcc.20035

[2] D. A. Case, T. E. Cheatham, T. Darden, H. Gohlke, R. Luo, K. M. Merz, A. Onufriev, C. Simmerling, B. Wang, R. J. Woods, The amber

biomolecular simulation programs, Journal of Computational Chemistry 26 (16) (2005) 1668–1688. doi:10.1002/jcc.20290.

URL http://dx.doi.org/10.1002/jcc.20290

[3] B. Xue, Q. Yang, Q. Zhang, X. Wan, D. Fang, X. Lin, G. Sun, G. Gobbo, F. Cao, A. M. Mathiowetz, B. J. Burke, R. A. Kumpf, B. K. Rai, G. P. F. Wood, F. C. I. Pickard, J. Wang, P. Zhang, J. Ma, Y. A. Jiang, S. Wen, X. Hou, J. Zou, M. Yang, Development and comprehensive benchmark of a high-quality amber-consistent small molecule force field with broad chemical space coverage for molecular modeling and free energy calculation, Journal of Chemical Theory and Computation 0 (0) (0) null, pMID: 38157475. arXiv:https://doi.org/10.1021/acs.jctc.3c00920, doi:10.1021/acs.jctc.3c00920.

URL https://doi.org/10.1021/acs.jctc.3c00920

[4] K. Vanommeslaeghe, E. Hatcher, C. Acharya, S. Kundu, S. Zhong, J. Shim, E. Darian, O. Guvench, P. Lopes, I. Vorobyov, A. D. Mackerell Jr., Charmm general force field: A force field for drug-like molecules compatible with the charmm all-atom additive biological force fields, Journal of Computational Chemistry 31 (4) (2010) 671–690. doi:https://doi.org/10.1002/jcc.21367.

URL https://onlinelibrary.wiley.com/doi/abs/10.1002/jcc.21367

[5] B. R. Brooks, R. E. Bruccoleri, B. D. Olafson, D. J. States, S. Swaminathan, M. Karplus, Charmm: A program for macromolecular energy, minimization, and dynamics calculations, Journal of Computational

41

Chemistry 4 (2) (1983) 187–217. doi:10.1002/jcc.540040211.

URL `http://dx.doi.org/10.1002/jcc.540040211`

[6] B. R. Brooks, C. L. Brooks III, A. D. Mackerell Jr., L. Nilsson, R. J. Petrella, B. Roux, Y. Won, G. Archontis, C. Bartels, S. Boresch, A. Caflisch, L. Caves, Q. Cui, A. R. Dinner, M. Feig, S. Fischer, J. Gao, M. Hodoscek, W. Im, K. Kuczera, T. Lazaridis, J. Ma, V. Ovchinnikov, E. Paci, R. W. Pastor, C. B. Post, J. Z. Pu, M. Schaefer, B. Tidor, R. M. Venable, H. L. Woodcock, X. Wu, W. Yang, D. M. York, M. Karplus, Charmm: The biomolecular simulation program, Journal of Computational Chemistry 30 (10) (2009) 1545–1614. doi:https://doi.org/10.1002/jcc.21287.

URL `https://onlinelibrary.wiley.com/doi/abs/10.1002/jcc.21287`

[7] W. L. Jorgensen, J. Tirado-Rives, The opls [optimized potentials for liquid simulations] potential functions for proteins, energy minimizations for crystals of cyclic peptides and crambin, Journal of the American Chemical Society 110 (6) (1988) 1657–1666, pMID: 27557051. arXiv:https://doi.org/10.1021/ja00214a001, doi:10.1021/ja00214a001.

[8] W. L. Jorgensen, D. S. Maxwell, J. Tirado-Rives, Development and testing of the opls all-atom force field on conformational energetics and properties of organic liquids, Journal of the American Chemical Society 118 (45) (1996) 11225–11236. arXiv:https://doi.org/10.1021/ja9621760, doi:10.1021/ja9621760.

[9] L.-P. Wang, T. J. Martinez, V. S. Pande, Building force fields: an auto-

matic, systematic, and reproducible approach, The journal of physical chemistry letters 5 (11) (2014) 1885–1891.

[10] Y. Qiu, D. G. A. Smith, C. D. Stern, M. Feng, H. Jang, L.-P. Wang, Driving torsion scans with wavefront propagation, The Journal of Chemical Physics 152 (24) (2020) 244116. doi:10.1063/5.0009232.
URL https://doi.org/10.1063/5.0009232

[11] J. T. Horton, S. Boothroyd, J. Wagner, J. A. Mitchell, T. Gokey, D. L. Dotson, P. K. Behara, V. K. Ramaswamy, M. Mackey, J. D. Chodera, J. Anwar, D. L. Mobley, D. J. Cole, Open force field bespokefit: Automating bespoke torsion parametrization at scale, Journal of Chemical Information and Modeling 62 (22) (2022) 5622–5633, pMID: 36351167.   arXiv:https://doi.org/10.1021/acs.jcim.2c01153, doi:10.1021/acs.jcim.2c01153.

[12] D. Mobley, C. C. Bannan, A. Rizzi, C. I. Bayly, J. D. Chodera, V. T. Lim, N. M. Lim, K. A. Beauchamp, M. R. Shirts, M. K. Gilson, P. K. Eastman, Open force field consortium: Escaping atom types using direct chemical perception with smirnoff v0.1, bioRxiv (2018). doi:10.1101/286542.
URL   https://www.biorxiv.org/content/early/2018/07/13/286542

[13] P. Eastman, J. Swails, J. D. Chodera, R. T. McGibbon, Y. Zhao, K. A. Beauchamp, L.-P. Wang, A. C. Simmonett, M. P. Harrigan, C. D. Stern, R. P. Wiewiora, B. R. Brooks, V. S. Pande, Openmm

7: Rapid development of high performance algorithms for molecular dynamics, PLOS Computational Biology 13 (7) (2017) 1–17. doi:10.1371/journal.pcbi.1005659.
URL `https://doi.org/10.1371/journal.pcbi.1005659`

[14] X. He, B. Walker, V. H. Man, P. Ren, J. Wang, Recent progress in general force fields of small molecules, Current Opinion in Structural Biology 72 (2022) 187–193. doi:https://doi.org/10.1016/j.sbi.2021.11.011.
URL `https://www.sciencedirect.com/science/article/pii/S0959440X21001603`

[15] C. I. Bayly, P. Cieplak, W. Cornell, P. A. Kollman, A well-behaved electrostatic potential based method using charge restraints for deriving atomic charges: the resp model, The Journal of Physical Chemistry 97 (40) (1993) 10269–10280. arXiv:https://doi.org/10.1021/j100142a004, doi:10.1021/j100142a004.

[16] A. Jakalian, D. B. Jack, C. I. Bayly, Fast, efficient generation of high-quality atomic charges. am1-bcc model: Ii. parameterization and validation, Journal of Computational Chemistry 23 (16) (2002) 1623–1641. doi:https://doi.org/10.1002/jcc.10128.
URL `https://onlinelibrary.wiley.com/doi/abs/10.1002/jcc.10128`

[17] P. Li, L. F. Song, K. M. J. Merz, Parameterization of highly charged metal ions using the 12-6-4 lj-type nonbonded model in explicit water, The Journal of Physical Chemistry B 119 (3) (2015)

883–895, pMID: 25145273. arXiv:https://doi.org/10.1021/jp505875v, doi:10.1021/jp505875v.

[18] R. Strickstrock, M. Hülsmann, D. Reith, K. N. Kirschner, Optimizing lennard-jones parameters by coupling single molecule and ensemble target data, Computer Physics Communications 274 (2022) 108285. doi:https://doi.org/10.1016/j.cpc.2022.108285.
URL https://www.sciencedirect.com/science/article/pii/S0010465522000030

[19] K. N. Kirschner, W. Heiden, D. Reith, Relative electronic and free energies of octane's unique conformations, Molecular Physics 115 (9-12) (2017) 1155–1165. arXiv:http://dx.doi.org/10.1080/00268976.2016.1262076, doi:10.1080/00268976.2016.1262076.

[20] Gestis-Stoffdatenbank, Properties of octan, accessed: 19. Jan 2024.
URL https://gestis.dguv.de/data?name=013810

[21] M. Hülsmann, T. Köddermann, J. Vrabec, D. Reith, Grow: A gradient-based optimization workflow for the automated development of molecular models, Computer Physics Communications 181 (3) (2010) 499 – 513. doi:https://doi.org/10.1016/j.cpc.2009.10.024.
URL http://www.sciencedirect.com/science/article/pii/S0010465509003452

[22] R. Strickstrock, Fflow github repository.

URL https://github.com/rstrickstrock/tuning_weighting-factors_objective-function.git

[23] H. Berendsen, D. van der Spoel, R. van Drunen, Gromacs: A message-passing parallel molecular dynamics implementation, Computer Physics Communications 91 (1-3) (1995) 43–56.
URL https://doi.org/10.1016/0010-4655(95)00042-E

[24] E. Lindahl, B. Hess, D. van der Spoel, Gromacs 3.0: a package for molecular simulation and trajectory analysis, Molecular modeling annual 7 (8) (2001) 306–317. doi:10.1007/s008940100045.
URL https://doi.org/10.1007/s008940100045

[25] K. Nabert, G. Schön (1963).

[26] NIST-Chemistry-Webbook, , accessed: 20. Feb 2024.
URL https://webbook.nist.gov/cgi/fluid.cgi?P=1&TLow=290.15&THigh=300.15&TInc=1&Digits=5&ID=C111659&Action=Load&Type=IsoBar&TUnit=K&PUnit=bar&DUnit=kg%2Fm3&HUnit=kcal%2Fmol&WUnit=m%2Fs&VisUnit=uPa*s&STUnit=N%2Fm&RefState=DEF

[27] O. Kunz, W. Wagner, The gerg-2008 wide-range equation of state for natural gases and other mixtures: An expansion of gerg-2004, Journal of Chemical & Engineering Data 57 (11) (2012) 3032–3091. arXiv:https://doi.org/10.1021/je300655b, doi:10.1021/je300655b.

[28] R. Beckmüller, M. Thol, I. H. Bell, E. W. Lemmon, R. Span, New Equations of State for Binary Hydrogen Mixtures Containing Methane, Nitrogen, Carbon Monoxide, and Carbon

46

Dioxide, Journal of Physical and Chemical Reference Data 50 (1) (2021) 013102. arXiv:https://pubs.aip.org/aip/jpr/article-pdf/doi/10.1063/5.0040533/14751783/013102_1_online.pdf, doi:10.1063/5.0040533.

URL `https://doi.org/10.1063/5.0040533`